

Model of two-phase flow dynamics for optimal water management in polymer electrolyte fuel cells

Chang-Hyun Yun, Yong-Chae Chung^a and Sung-Chul Yi*

Department of Chemical Engineering, Hanyang University, Seoul 133-791, Korea

^aDepartment of Materials Science and Engineering, Hanyang University, Seoul 133-791, Korea

A three-dimensional, mathematical model for two-phase flow dynamics in polymer electrolyte fuel cells has been developed based on the two-flow model and the mist flow model. Our proposed model basically consists of three zones to account for water flow dynamics: (i) a single-phase flow zone in the gas channel, (ii) two-phase flow zones in the catalyst layer and the gas diffusion layer, and (iii) an electrolyte-phase flow zone in the electrolyte membrane. The mist flow model and the two-flow model are applied to single-phase and two-phase flow zones, respectively. The model employed in this research focuses on water management that balances membrane dehydration with electrode flooding. From the simulation results, it can be concluded that the optimal operating conditions are the inlet humidification level of 100% anode and 50% cathode at 70 °C and the anode and cathode inlet stoichiometry ratio of 1.8 at 1.5 A/cm² reference current density.

Key words: PEFC, Modeling, Two-Phase Transport, Water Management, CFD.

Introduction

Water flooding is one of the main limitations in polymer electrolyte fuel cells (PEFCs) performance. This is a phenomenon that liquid-phase water generated in the cathode catalyst layer by electrochemical reactions condenses and blocks some of the open pores, limiting the mass transport of oxygen to the catalyst layer through the gas diffusion layer. Additionally, liquid-phase water covers the active sites on catalysts, decreasing the electrochemically-active surface area. Consequently, water flooding results in a serious problem that reduces the cell performance by the limitation of the oxygen reduction reaction. On the other hand, water is an important factor for the hydration of the membrane which is required for high proton conductivity. A polymer membrane used in a PEFC, as an electrolyte, must be sufficiently wetted by water to maintain a high proton conductivity. Therefore, effective water management is an essential problem to be solved for enhancing cell performance.

However, an experimental understanding of the water transport phenomena involving water flooding is limited by the inaccessibility of *in situ* experimental measurements for PEFC electrodes and the following complex mechanisms of water transport across the membrane phase: (i) electro-osmotic drag due to the proton flux, (ii) permeation due to the hydraulic pressure

gradient, and (iii) diffusion due to the concentration gradient. And numerical simulations on PEFCs continue to gain acceptance as an essential tool to overcome this limitation.

Many researchers have made significant attempts to develop mathematical models for two-phase flow dynamics in PEFCs. Early efforts were made by Springer et al. [1, 2].

They proposed a one-dimensional model for predicting PEFC performance. This model predicted the water flooding effect on cell performance, but didn't consider the liquid water transport by a flooding parameter. A more realistic and detailed model is the two-flow model of Nguyen et al. [3, 4]. They presented a two-dimensional, water two-phase model included capillary transport of liquid water in the gas diffusion layer. However, this model considered only the cathode regions for an analysis of the water flooding effect. More recently, Pasaogullari and Wang [5] developed a three-dimensional, two-phase model of a PEFC based on a multiphase mixture formulation by Wang and Cheng [6]. This model considered all regions of the PEFC. However, the water activity in the two-phase zone was unreasonably significant and analysis of liquid water transport in the anode regions is very unstable.

The objective of the present study is to develop a three-dimensional mathematical model which includes the two-phase flow dynamics of PEFCs, thereby predicting the water flood phenomena. The present model is fundamentally based on the two-flow model [3, 4] and the mist flow model [5]. The mist flow model is applied in the gas channels on the assumption that two-phase mist flow is present inside the gas channels and

*Corresponding author:
Tel : +82-2-2220-0481
Fax: +82-2-2298-5147
E-mail: scyi@hanyang.ac.kr

the liquid velocity is equivalent to the gas velocity. And the two-flow model is applied in the catalyst layers and gas diffusion layers. In addition, the effects of the inlet humidification level and stoichiometry ratio on cell performance were investigated and optimal conditions of water management were found.

Mathematical Model

Model Description

Figure 1 shows a scheme of a three-dimensional PEFC system. In this research the system was considered a serpentine, 35-flow-channeled unit cell system. The modelled regions consist of two flow channels, two gas diffusion layers, two catalyst layers and an electrolyte membrane. Fully humidified H_2 and air at $70^\circ C$ are supplied to the anode and cathode inlet channel, respectively. Water is generated at the cathode catalyst layer by the oxygen reduction reaction. However, if too much water accumulates in the cathode, it condenses and may result in water flooding.

Model assumptions

The proposed model includes the following assumptions: (i) ideal gas mixtures, (ii) incompressible and laminar flow, (iii) a homogeneous porous gas diffusion layer and catalyst layer, (iv) isothermal cell condition, (v) a highly electron-conductive solid matrix, and (vi) mist flow condition of liquid water inside channels.

Governing equations

The mass conservation equation is:

$$\nabla \cdot (\rho \mathbf{u}) = 0 \quad (1)$$

where ρ is the density of the gas phase. According to the preceding assumption (ii), mass source/sink terms are ignored.

The momentum conservation equation is:

$$\frac{1}{(\varepsilon^{eff})^2} \nabla \cdot (\rho \mathbf{u} \mathbf{u}) = -\nabla P + \nabla \cdot (\mu \nabla \mathbf{u}) + S_u \quad (2)$$

where ε is the effective porosity inside porous mediums, and μ is the viscosity of the gas phase.

The momentum source term, S_u , is used to describe Darcy's drag for flow through porous gas diffusion layers and catalyst layers [7, 8] as:

$$S_u = -\frac{\mu}{K} \mathbf{u} \quad (3)$$

where K is the gas permeability inside porous mediums.

The species conservation equation is:

$$\nabla \cdot (\mathbf{u} C_k) = \nabla \cdot (D_k^{eff} \nabla C_k) + S_k \quad (4)$$

where D_k^{eff} is the effective diffusion coefficient of species k (e.g. hydrogen, oxygen, nitrogen and water vapor) and is defined to describe the effects of porosity in the porous gas diffusion layers and catalyst layers by the Bruggeman correlation [9] as:

$$D_k^{eff} = (\varepsilon^{eff})^{1.5} D_k \quad (5)$$

In addition, the diffusion coefficient is defined as a function of temperature and pressure [10] by the following equation:

$$D_k = D_k^0 \left(\frac{T}{T_0} \right)^{3/2} \left(\frac{P_0}{P} \right) \quad (6)$$

Transport properties for species are summarized in Table 1.

The charge conservation equation is:

$$\nabla \cdot (\kappa_e^{eff} \nabla \Phi_e) + S_\Phi = 0 \quad (7)$$

where κ_e is the proton conductivity in the membrane phase and has been correlated by Springer et al. [1] as:

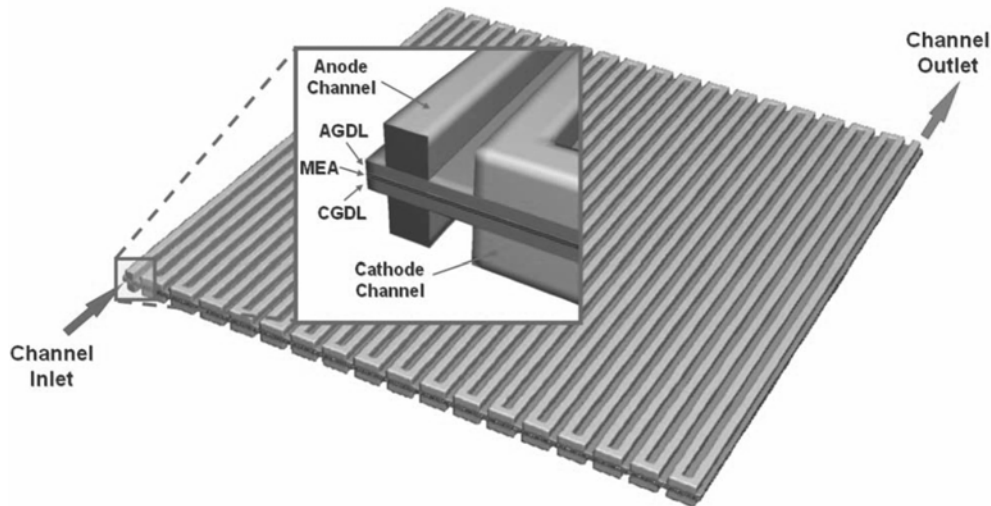


Fig. 1. A schematic of the unit cell of PEFC.

Table 1. Transport properties [7, 10]

Property	Value
H_2 diffusivity in the gas channel, $D_{H_2}^0$	$1.1028 \times 10^{-4} \text{ m}^2/\text{s}$
O_2 diffusivity in the gas channel, $D_{O_2}^0$	$3.2048 \times 10^{-5} \text{ m}^2/\text{s}$
H_2O diffusivity in the gas channel, $D_{H_2O}^0$	$7.35 \times 10^{-5} \text{ m}^2/\text{s}$
H_2 diffusivity in the membrane, $D_{H_2}^{mem}$	$2.59 \times 10^{-10} \text{ m}^2/\text{s}$
O_2 diffusivity in the membrane, $D_{O_2}^{mem}$	$1.22 \times 10^{-10} \text{ m}^2/\text{s}$

$$\kappa_e = (0.005139\lambda - 0.00326) \exp\left(1268 \left(\frac{1}{303} - \frac{1}{T}\right)\right) \quad (8)$$

where λ is the water content of the membrane phase, which means the number of water molecules per sulfonate group inside the membrane phase. The water content is defined as a function of the water activity, a , by the following fit of the experimental data [11]:

$$\lambda = 0.3 + 6a[1 - \tanh(a - 0.5)] + 3.9\sqrt{a} \left[1 + \tanh\left(\frac{a - 0.89}{0.23}\right) \right] \quad (9)$$

Here, the water activity, a , is given by [12]:

$$a = \frac{C_w RT}{P_w^{sat}} + 2s \quad (10)$$

where $2s$ is added to the original formulation to account for the phase change in the present two-phase model. By the Bruggeman correlation [9], the proton conductivity in the catalyst layers is defined as:

$$\kappa_e^{eff} = \varepsilon_m^{1.5} \kappa_e \quad (11)$$

where ε_m is the volume fraction of the membrane-phase in the catalyst layer.

The source/sink term, S_k and S_Φ , in Eq. (4) and (7) are given in Table 2.

Using the electrolyte-phase potential, Φ_e , obtained by Eq. (7), it is possible to calculate the electrolyte-phase potential gradient in the membrane. Finally, the local current densities are obtained by:

$$I = -\kappa_e \nabla \Phi_e \quad (12)$$

Table 2. Source terms for species and charge conservation equations in each regions

	Species	Charge
Flow channels	$S_k = 0$	$S_\Phi = 0$
Gas diffusion layers	$S_k = 0$	$S_\Phi = 0$
Catalyst layers	$S_k = -\nabla \cdot \left(\frac{n_d I}{F} \right) - \frac{S_{kl}}{nF}$	$S_\Phi = j$
Membrane	$S_k = -\nabla \cdot \left(\frac{n_d I}{F} \right)$	$S_\Phi = 0$

The average current density is then calculated from:

$$I_{avg} = \frac{1}{A_{mem}} \int_{A_{mem}} I dA \quad (13)$$

Water transport

The present model basically consists of three zones to account for water flow dynamics: (i) a single-phase flow zone in the gas channel, (ii) two-phase flow zones in the gas diffusion layer and the catalyst layer, and (iii) an electrolyte-phase flow zone in the electrolyte membrane.

The mist flow model [5] and the two-flow model [3, 4] are applied to the single-phase and two-phase flow zones, respectively.

– The water transport in the electrolyte membrane

The water transport in the membrane is defined as the following conservation equation:

$$\nabla \cdot (D_{H_2O}^{mem} \nabla D_{H_2O}^{mem}) - \nabla \cdot \left(\frac{n_d}{F} \mathbf{i} \right) = 0 \quad (14)$$

where $D_{H_2O}^{mem}$ and n_d are the water diffusivity and the electro-osmotic drag coefficient in the membrane phase, respectively and are obtained by the following fits of the experimental data [11]:

$$D_{H_2O}^{mem} = 4.1 \times 10^{-10} \left(\frac{\lambda}{25} \right)^{0.15} \left[1 + \tanh\left(\frac{\lambda - 2.5}{1.4}\right) \right] \quad (15)$$

$$n_d = \begin{cases} 1 & \lambda < 9 \\ 0.117\lambda - 0.0544 & \lambda \geq 9 \end{cases} \quad (16)$$

The equivalent water concentration, $C_{H_2O}^{mem}$, is given by:

$$C_{H_2O}^{mem} = \frac{\rho_{mem} \lambda}{EW} \quad (17)$$

where ρ_{mem} and EW are the dry membrane density and the equivalent weight of the membrane, respectively.

In this study, the permeation of liquid water due to the hydraulic pressure gradient across the membrane has been neglected, because the hydraulic permeability and pressure gradient is very small in the membrane.

– Liquid water transport

The liquid water conservation equation is:

$$\nabla \cdot (\rho_l \mathbf{u}_l s) = -\nabla \cdot \left(\rho_l \frac{Ks^3}{\mu_l} \frac{dp_e}{ds} \nabla s \right) + S_w \quad (18)$$

where ρ_l and μ_l are the density and viscosity of the liquid phase, respectively. The water saturation, s , is the volume fraction of liquid water inside the open pore space of the gas diffusion layers and catalyst layers.

In the present model, it is assumed that the liquid

phase velocity, \mathbf{u}_l , in the gas channel is equal to the gas phase velocity according to the mist flow model that the liquid water in the gas channel is assumed to exist in a fine mist and travel with the gas velocity.

The liquid water transport in the porous gas diffusion layers and the catalyst layers is influenced by the capillary pressure. The definition of the capillary pressure, p_c , is:

$$p_c = P - p_l \quad (19)$$

where P and p_l are the pressure of the gas phase and liquid phase, respectively. In this study, the capillary pressure is related to phase saturations via the Leverette function [13] as:

$$p_c = \sigma \left(\frac{\varepsilon}{K} \right)^{1/2} \cos(\theta_c) J(s) \quad (20)$$

where σ is the surface tension, θ_c is the contact angle and $J(s)$ is the Leverette function, and is given by:

$$J(s) = \begin{cases} 1.417(1-s) - 2.120(1-s)^2 + 1.263(1-s)^3 & \text{if } \theta_c < 90^\circ \\ 1.417s - 2.120s^2 + 1.263s^3 & \text{if } \theta_c > 90^\circ \end{cases} \quad (21)$$

The source/sink term, S_w , in Eq. (18) is defined as:

$$S_w = \begin{cases} k_c \varepsilon^{eff} x_w \left(C_w - \frac{P_w^{sat}}{RT} \right) M_{H_2O} & \text{if } C_w > C_w^{sat} \\ -k_e \varepsilon_0 \rho_l \left(\frac{P_w^{sat}}{RT} - C_w \right) & \text{if } C_w < C_w^{sat} \end{cases} \quad (22)$$

where k_c and k_e are the condensation and evaporation rate constants, respectively. C_w is the molar concentration of water vapor. The saturation pressure of water, P_w^{sat} , can be computed from Springer et al. [1] by the following equation:

$$\log_{10} P_w^{sat} = -2.1794 + 0.02953(T - 273.15) - 9.1837 \times 10^{-5} (T - 273.15)^2 + 1.4454 \times 10^{-7} (T - 273.15)^3 \quad (23)$$

The source/sink term of the liquid water conservation equation is not applied in gas channels according to the mist flow assumption.

- Water flooding

Liquid water generated in the cathode catalyst layer by an electrochemical reaction condenses and blocks some of the open pores, limiting the mass transport of oxygen to the catalyst layer through the gas diffusion layer. In the present model, this effect is employed by:

$$\varepsilon^{eff} = \varepsilon_0 (1-s) \quad (24)$$

Additionally, liquid-phase water covers the active sites

Table 3. Material properties [15, 16]

Property	Value
Gas diffusion layer porosity, ε_{GDL}	0.4
Volume fraction of membrane in catalyst layer, ε_m	0.5
Dry membrane density, ρ_{mem}	1980 kg/m ³
Equivalent weight of membrane, EW	1.1 kg/mol
Surface tension, σ	0.0625 N/m
Contact angle of gas diffusion layer, θ_c	110°

on catalysts, decreasing the electrochemically-active surface area. This is modeled as:

$$a^{eff} = a_0 (1-s) \quad (25)$$

Detailed material properties are given in Table 3.

Electrochemical kinetics

The exchange current density, j , means the transfer current between the solid-phase matrix and the electrolyte-phase in the catalyst layers. In the anode catalyst layer, the hydrogen oxidation reaction (HOR), which has much faster kinetics relatively than the oxygen reduction reaction (ORR), which can be defined by the following linear electro-chemical kinetic rate equation [1]:

$$j_a = a^{eff} j_a^{ref} \left(\frac{C_{H_2}}{C_{H_2}^{ref}} \right)^{1/2} \left(\frac{\alpha_a + \alpha_c}{RT} F \eta \right) \quad (26)$$

where α_a and α_c are the anode and cathode transfer coefficients, respectively and the sum of these is preferred to be 2. In the cathode catalyst layer, the oxygen reduction reaction (ORR) is defined by the following Tafel kinetic rate equation:

$$j_c = -a^{eff} j_c^{ref} \left(\frac{C_{O_2}}{C_{O_2}^{ref}} \right) \exp \left(-\frac{\alpha_c}{RT} F \eta \right) \quad (27)$$

where the cathode transfer coefficient, α_c , is taken to be unity. The overpotential, η , is given by:

$$\eta = \Phi_s - \Phi_e - V_{oc} \quad (28)$$

According to the preceding assumption (v), Φ_s is equal to zero in the anode catalyst layer and to the cell voltage in the cathode catalyst layer. The thermodynamic open circuit potential, V_{oc} , becomes zero for the anode and is defined for the cathode as [14]:

$$V_{oc} = 1.23 - 0.9 \times 10^{-3} (T - 298.15) \quad (29)$$

Detailed electrochemical properties are given in Table 4.

Boundary conditions

For the momentum conservation equation, gas velocities are specified at each inlet of the anode and cathode flow channels. The velocity is calculated based

Table 4. Electrochemical properties

Property	Value
Anode reference exchange current density, $a_0 J_a^{ref}$	1.0×10^9 A/m ³
Cathode reference exchange current density, $a_0 J_c^{ref}$ at 343.15 K	1.8×10^3 A/m ³
Faraday constants, F	96487 C/mol
Universal gas constant, R	8.314 J/mol K

on the concept of stoichiometry, ζ , which means the required amount of fuel at a given current. Then, the inlet velocities for the anode and cathode inlets are expressed by:

$$\mathbf{u}_{in,a} = \frac{\zeta_a I_{ref} A_{MEA}}{2 C_{H_2,in} F A_{ch}}, \quad \mathbf{u}_{in,c} = \frac{\zeta_c I_{ref} A_{MEA}}{4 C_{O_2,in} F A_{ch}} \quad (30)$$

where I_{ref} is the reference current density, and A_{MEA} and A_{ch} are the electrode surface and the flow channel area, respectively. The inlet species concentrations are calculated by the anode and cathode humidification conditions.

At each outlet of the anode and cathode flow channels, fully developed flow is assumed with back pressure and species concentrations are given by a no-flux boundary condition.

Numerical implementation

In this study, numerical modeling and simulation of a three dimensional PEFC were implemented with a commercially available computational fluid dynamics code, FLUENT, by customizing via user-defined functions. Over 500 iterations, about 3 hours were taken to reduce each residual value below 10^{-8} with a 3.0 GHz PC. About 800,000 computational cells were used in all the simulations.

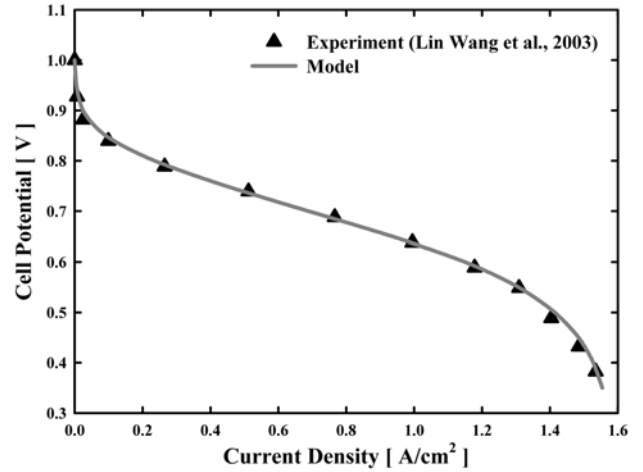
Results and Discussion

Model validation

To validate the present model, a comparison with experimental data [15] has been carried out. The dimensions of the model are given in Table 5, based on a realistic experimental cell geometry. For the validation, the operational conditions are specified as 70 °C and 3 atm for both the anode and cathode, and inlet species are fully humidified at 70 °C. The flow rates for the

Table 5. Dimensions of PEFC [15]

Dimension	Value
Gas channel length	7.0×10^{-2} m
Gas channel width and depth	1.0×10^{-3} m
Gas diffusion layer thickness	3.0×10^{-4} m
Catalyst layer thickness	1.29×10^{-5} m
Membrane thickness	1.08×10^{-4} m


Fig. 2. Measured and calculated average polarization curves at 70 °C and 3 atm, fully humidified inlets at 70 °C, and anode/cathode stoichiometry ratio of 1.8/1.4 at 1.5 A/cm².

anode and cathode inlet have constant values corresponding to a stoichiometric flow ratio of 1.8 and 1.4 at the reference current density of 1.5 A/cm², respectively.

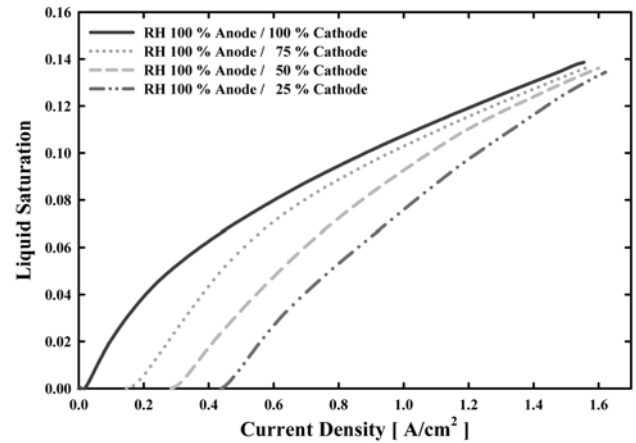
Figure 2 compares the polarization curve predicted with the experimental data. Note the coincidence of the experimental data and the model.

Through the present model, the following parametric studies were performed to gain the optimal water management conditions.

The Effect of inlet humidification level on cell performance

To investigate the effect of inlet humidification conditions on water flooding, simulations were performed at various humidification levels. The relative humidity of the cathode inlet varied from 25 to 100% at 70 °C, and the anode was fixed by 100%. The other operational conditions were equal to the preceding validation case.

Figure 3 and 4 display the average liquid saturation levels in the cathode catalyst layer and the polarization


Fig. 3. Predicted average liquid saturation levels in the cathode catalyst layer for different inlet humidification levels.

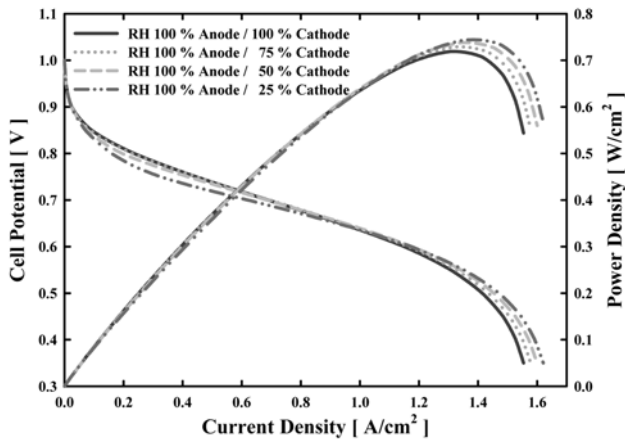


Fig. 4. Calculated average polarization and power curves for different inlet humidification levels.

and power curves for different humidification levels, respectively. In the fully humidified case, liquid water exists even at low current densities and gradually increases as the current density increases, due to an increase in the water production rate in the cathode catalyst layer. When the average current density ranges beyond 1.3 A/cm^2 , the polarization curve rapidly declined due to the mass transport limitation and water flooding. In the case of 100% anode and 25% cathode, liquid water is not present below 0.3 A/cm^2 because the water vapor concentration is smaller than the saturation level in this range. When the average current density ranges below 0.8 A/cm^2 , the cell performance is significantly lower than the fully humidified case due to the relatively low hydration of the membrane. However, beyond 0.9 A/cm^2 , the average current density is significantly higher than the fully humidified case. This result arises from three main factors: (i) complete hydration of the membrane by water produced from the ORR, (ii) a relatively low water flooding level, and (iii) a relatively higher inlet molar concentration of oxygen due to the low inlet relative humidity.

From the results of the inlet humidification effect on the cell performance, it can be concluded that the optimal inlet humidification level is at 100% anode and 50% cathode where the optimal cell performance was seen throughout the average polarization and power curves.

The Effect of the inlet stoichiometry ratio on cell performance

Generally, high inlet stoichiometry conditions enhance the cell performance as they relieve the mass transport limitation of oxygen at high current densities. However, high stoichiometry conditions adversely affect the cell performance due to drying out of the membrane, especially in low humidity conditions. Furthermore, high stoichiometry conditions reduce the overall system efficiency due to an increase in the air compressor load. In this part, a simulation is performed on the

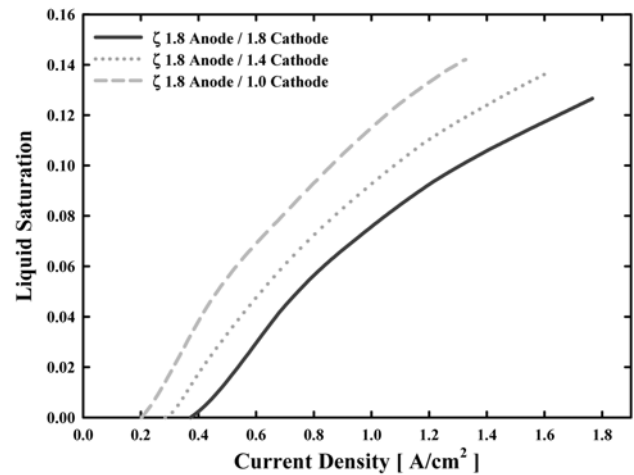


Fig. 5. Predicted average liquid saturation levels in the cathode catalyst layer for different inlet stoichiometry ratios.

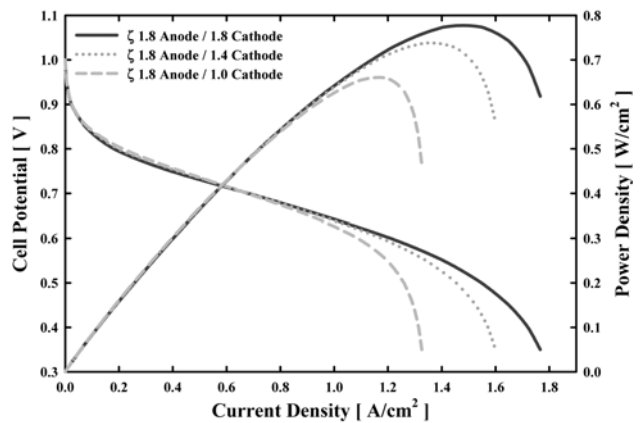


Fig. 6. Calculated average polarization and power curves for different inlet stoichiometry ratios.

various inlet stoichiometry ratios to investigate the effect of inlet stoichiometry conditions on the cell performance. The stoichiometry ratio of the cathode inlet varied from 1.0 to 1.8 at 1.5 A/cm^2 reference current density and the anode was fixed by 1.8. The other operational conditions are equal to the relative humidity case of 100% anode and 50% cathode performed in the previous part.

Figure 5 and 6 show the average liquid saturation levels in the cathode catalyst layer, and the polarization and power curves for different inlet stoichiometry ratios, respectively. In the average current density region below 0.5 A/cm^2 , the cell performance was slightly higher when the stoichiometry ratio was lower because the water concentration in the flow channel increased faster and the membrane was hydrated better.

However, in the average current density region beyond 1.0 A/cm^2 , the average polarization curve of the lower inlet stoichiometry case declines much faster than the higher stoichiometry case, due to the faster mass transport limitation. Moreover, as shown in Fig. 5, liquid water was produced faster and more in the lower

stoichiometry condition due to the rapid increase of the water concentration in the flow channel, resulting in a decline of the cell performance.

Finally, from the preceding results of the inlet stoichiometric and humidification effect on the cell performance, it can be concluded that the optimal operating conditions are an inlet humidification level of 100% anode and 50% cathode at 70 °C and the inlet stoichiometry ratio of 1.8 anode and 1.8 cathode at 1.5 A/cm² reference current density.

Conclusions

A three-dimensional, mathematical model for two-phase flow dynamics in polymer electrolyte fuel cells has been developed based on the two-flow model and the mist flow model. From a comparison with experimental polarization curve data [15], the model is validated. To obtain the optimal operating conditions on water management, detailed analyses of the inlet stoichiometric and humidification effect on the cell performance were performed. Consequently, it can be concluded that the optimal operating conditions are an inlet humidification level of 100% anode and 50% cathode at 70 °C and the anode and cathode inlet stoichiometry ratio of 1.8 at 1.5 A/cm² reference current density.

Acknowledgement

This work is supported by the research fund of Hanyang University (2004) and the authors gratefully appreciate the financial support.

Nomenclature

List of symbols

a	: water activity
a_0	: specific surface area [1/m]
A	: area [m ²]
$AGDL$: anode gas diffusion layer
C	: molar concentration [mol/m ³]
D	: diffusion coefficient [m ² /s]
EW	: equivalent weight of membrane
F	: Faraday constant [C/mol]
I	: local current density [A/m ²]
j	: exchange current density [A/m ²]
k_c	: condensation rate constant
k_e	: evaporation rate constant
K	: gas permeability [m ²]
n_d	: electro-osmotic drag coefficient
p_c	: capillary pressure [Pa]
P	: pressure [Pa]
R	: universal gas constant [J/mol·K]
RH	: relative humidity
s	: saturation
S	: source/sink term

T	: temperature [K]
u	: velocity [m/s]
V_{oc}	: open-circuit potential [V]

Greek Letters

α	: transfer coefficient
ε	: porosity
Φ	: potential [V]
η	: local overpotential [V]
κ	: proton conductivity [S/m]
λ	: water content
μ	: viscosity [kg/m·s]
θ_c	: contact angle [°]
ρ	: density [kg/m ³]
σ	: surface tension [N/m]
ζ	: stoichiometry ratio

Superscripts

eff	: effective
ref	: reference

Subscripts

a	: anode
avg	: average
c	: cathode
ch	: flow channel
e	: electrolyte-phase
GDL	: gas diffusion layer
in	: inlet
k	: species
l	: liquid
m	: membrane-phase in the catalyst layer
mem	: membrane
MEA	: membrane electrode assembly
s	: solid-phase
u	: momentum
w	: water

References

1. T.E. Springer, T.A. Zawodzinski, and S. Gottesfeld, J. Electrochem. Soc. 138[8] (1991) 2334-2342.
2. T.E. Springer, M.S. Wilson, and S. Gottesfeld, J. Electrochem. Soc. 140[12] (1993) 3513-3526.
3. W. He, J.S. Yi, and T.V. Nguyen, AIChE Journal 46[10] (2000) 2053-2064.
4. D. Natarajan, and T.V. Nguyen, J. Electrochem. Soc. 148[12] (2001) A1324-A1335.
5. U. Pasaogullari, and C.Y. Wang, J. Electrochem. Soc. 152[2] (2005) A380-A390.
6. C.Y. Wang, and P. Cheng, Adv. Heat Transfer 30 (1997) 93-196.
7. D.M. Bernardi, and M.W. Verbrugge, J. Electrochem. Soc. 139[9] (1992) 2477-2491.
8. V. Gurau, H. Liu, and S. Kakac, AIChE J. 44[11] (1998) 2410-2422.
9. R.E. Meredith, and C.W. Tobias, Advances in Electrochemistry and Electrochemical Engineering 2, Tobias, C. W., ed., Interscience Publishers, New York (1962).

10. R.B. Bird, W.E. Stewart, and E.N. Lightfoot, *Transport Phenomena*, John Wiley, New York (1960).
11. A.A. Kulikovskiy, *J. Electrochem. Soc.* 150[11] (2003) A1432-A1439.
12. M.E. Brandon, "One Dimensional, Transient Model of Heat, Mass, and Charge Transfer in a Proton Exchange Membrane" (M.S. Thesis, Mechanical Engineering, Virginia Polytechnic and State University, Blacksburg, VA, USA, 2001).
13. M.C. Leverette, *AIME Trans.* 142 (1941) 152-169.
14. C. Berger, *Handbook of Fuel Cell Technology*, Prentice-Hall, NJ. (1968).
15. L. Wang, A. Husar, T. Zhou, and H. Liu, *Int. J. Hydrog. Energy* 28[11] (2003) 1263-1272.
16. J.S. Lee, N.D. Quan, J.M. Hwang, S.D. Lee, H. Kim, H. Lee, and H.S. Kim, *J. Ind. Eng. Chem.* 12[2] (2006) 175-183.